

Time-resolved near-field optics: exciton transport in semiconductor nanostructures

A. RICHTER,* M. SÜPTITZ,* CH. LIENAU,* T. ELSAESSER,* M. RAMSTEINER,† R. NÖTZEL† & K. H. PLOOG†

*Max-Born-Institut für Nichtlineare Optik und Kurzzeitspektroskopie, D-12489 Berlin, Germany,

†Paul-Drude-Institut für Festkörperelektronik, D-10117 Berlin, Germany

Key words. Exciton transport, GaAs, near-field microscopy, low temperatures, luminescence spectroscopy, picosecond time resolution, quantum wire.

Summary

We present a systematic, temperature-dependent study of excitonic real-space transfer into single GaAs quantum wires using time-resolved low-temperature near-field luminescence spectroscopy. Excitons generated by local short pulse optical excitation in a 250 nm spot undergo diffusive transport over a length of several micrometres and are subsequently trapped into the quantum wire by optical phonon emission. The effect of local energy barriers in the vicinity of the quantum wire on the real-space transfer dynamics is monitored directly by mapping the time-resolved quantum wire luminescence. Experiments at variable temperatures are compared to numerical simulations based on drift-diffusive model calculations, and the spatio-temporal evolution of the two-dimensional exciton distribution within the nanostructure is visualized.

Introduction

Time-resolved far-field spectroscopic experiments provide direct insight into the dephasing, scattering and energy relaxation of free carrier and excitonic wavepackets in semiconductor nanostructures and are the experimental basis for a detailed theoretical description of these processes. In general, however, such studies give less direct information on the ballistic and diffusive real-space transfer of photogenerated carriers or their trapping into low-dimensional nanostructures, processes that involve the real-space motion of carriers on typical length scales of 10–1000 nm, beyond the spatial resolution that is attained with conventional far-field spectroscopy. In contrast, near-field scanning optical microscopy (NSOM) (Pohl *et al.*, 1984, Betzig & Trautman, 1992) overcomes the diffraction-limited

resolution of classical microscopy and offers subwavelength spatial resolution in the 100 nm range. In combination with time-resolved excitation and detection schemes, it gives direct access to carrier dynamics on ultrashort time and length scales. This has been demonstrated in spatially-resolved pump and probe experiments on GaAs microdiscs (Stark *et al.*, 1996) and in a study of exciton spin dynamics in magnetic heterostructures (Levy *et al.*, 1996).

In this report, we combine low-temperature near-field scanning optical microscopy and time-resolved luminescence spectroscopy. We study systematically the real-space transfer of excitons and the subsequent trapping into a single quasi-one-dimensional nanostructure, a quantum wire (QWR), over a wide temperature range between 10 K and 100 K. The high spatial resolution of 250 nm and the time resolution of 260 ps allow a detailed analysis of the microscopic carrier dynamics in real-space. Comparing experimental results and theoretical model calculations, we demonstrate the pronounced influence of the lateral confinement potential of the nanostructure on the exciton transport properties.

The investigated QWR structure and the experimental arrangement are shown schematically in Fig. 1. The sample was grown by molecular beam epitaxy on patterned GaAs (311)A substrates at the sidewall of 15–20 nm high mesa stripes orientated along [01–1] (Nötzel *et al.*, 1996). It consists of a nominally 6-nm thick GaAs quantum well (QW) layer clad by 50-nm thick $\text{Al}_{0.5}\text{Ga}_{0.5}\text{As}$ barriers. In the growth process, formation of a sidewall QWR arises from the preferential migration of Ga atoms within the QW layer from both the mesa top and the mesa bottom towards the sidewall, resulting in a local increase of the GaAs QW thickness. This change in QW thickness leads to a quasi-one-dimensional (1D) confinement over a lateral width of 50 nm. The lateral confinement potential of this QWR, plotted in Fig. 2, was derived from low-temperature photoluminescence excitation measurements with a spatial

Correspondence to: Ch. Lienau. E-mail: lienau@mbi-berlin.de
PACS numbers: 78·66.Fd, 78·55.Cr

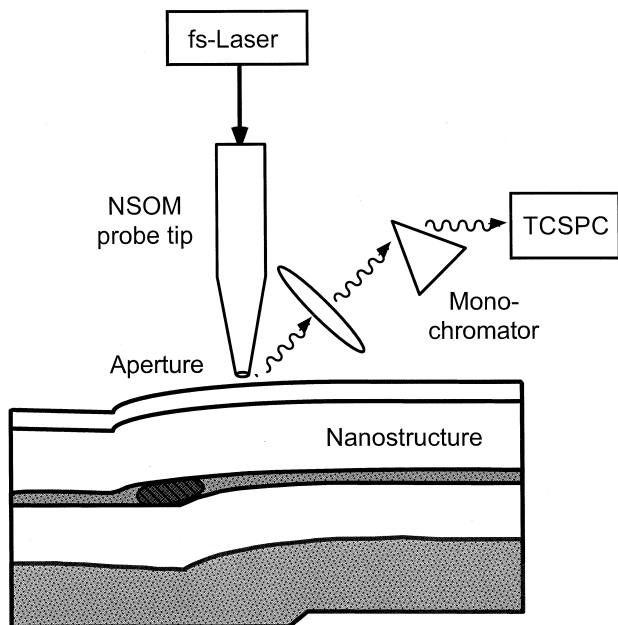


Fig. 1. Schematic of the experimental set-up and the sidewall quantum wire structure. Temporally and spatially resolved excitation of the sample is achieved by transmitting light from a femtosecond Ti:sapphire laser through a nanometer-sized aperture at the end of a near-field fibre probe. Photoluminescence is collected with a far-field microscope, spectrally resolved in a double monochromator and detected with a Si avalanche photodiode using the time-correlated single photon counting technique. The sample is mounted on an *xyz*-stage and scanned relative to the tip.

resolution of 250 nm (Richter *et al.*, 1997, Lienau *et al.*, 1998). These experiments, performed with the same near-field probes as used in the present study, give local variations of the bandgap of the embedding QW along the *y* direction,

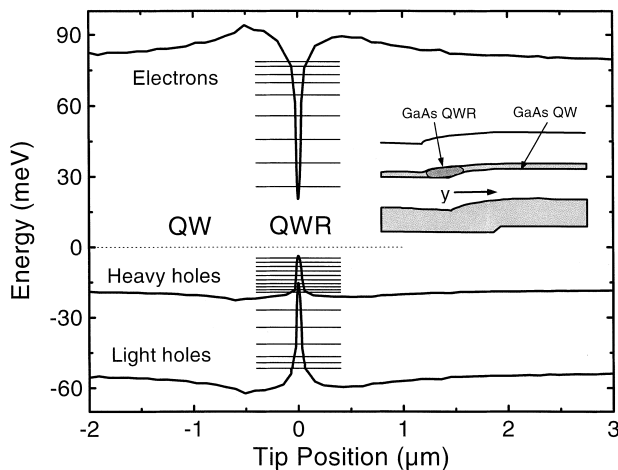


Fig. 2. Lateral confinement potential of the quantum wire (QWR) structure, as derived from spatially-resolved low-temperature photoluminescence excitation measurements. The horizontal lines indicate the calculated subband energies.

that is, perpendicular to the QWR. On the mesa bottom ($y < 0$), the QW band gap increases by up to 18 meV over a length of 2 μm , representing a barrier for lateral carrier motion. On the mesa top ($y > 0$) the bandgap shift is smaller and amounts to about 14 meV. The maxima of the two barriers separating QWR and flat area QW have a lateral distance of 800 nm. The change in bandgap energy originates from a local change in QW thickness (Lienau *et al.*, 1998). Within the experimental accuracy, the same spatial bandgap profile was found for different positions on the sample.

In this structure, carrier transport is studied at variable cryogenic temperatures by time-resolved near-field spectroscopy using a near-field scanning optical microscope (Behme *et al.*, 1997). Carriers are locally excited in the QW by transmitting a short optical pulse from a mode-locked Ti:sapphire laser through a metal-coated fibre near-field probe of 200 nm diameter (Betzig *et al.*, 1991). The photogenerated carriers undergo real-space transfer within the nanostructure and are eventually trapped into the 1D states of the QWR. The carrier migration time from the point of generation towards the QWR is monitored via the time-resolved onset of QWR luminescence. The 16 meV broad spectrum of the laser is centred at 1.614 eV and overlaps the excitonic absorption band of the QW. QWR photoluminescence (PL) at 1.54 eV, the maximum of the QWR PL spectrum, is collected in the far-field by a microscope objective. The luminescence is dispersed in a 0.22-m double monochromator (resolution $\Delta\lambda = 1.2$ nm) and detected with a silicon avalanche photodiode using time-correlated single photon detection with a temporal resolution of 260 ps. The single photon counting electronics is synchronized with the scanning electronics and luminescence decay curves are accumulated for each of 100 excitation positions, separated by 100 nm, while scanning the fibre probe perpendicular to the wire axis. The laser power on the sample was 10–100 nW, corresponding to very low excitation densities between 10^4 and 10^5 cm^{-2} .

First, experiments at a temperature of 100 K are discussed. We know from stationary PL experiments that, in this temperature range, electron-hole pairs are effectively trapped into the QWR that are generated up to distances of several micrometres from the QWR within the embedding QW (Lienau *et al.*, 1998). Moreover, the energy of the potential barriers separating QWR and QW is similar to the thermal energy at this temperature so that we expect a considerable influence of the barrier potential on the carrier dynamics. In Fig. 3, the intensity of the time-resolved QWR emission is shown as a function of tip position along the lateral *y*-axis (abscissa) and delay time (ordinate). The QWR is located at $y = 0$. Cross-sections through Fig. 3, i.e. the time evolution of the luminescence for fixed excitation positions $|y| = 0, 0.4, 1$ and 2 μm are shown in Fig. 4(a) and (b), for excitation on mesa top and mesa bottom,

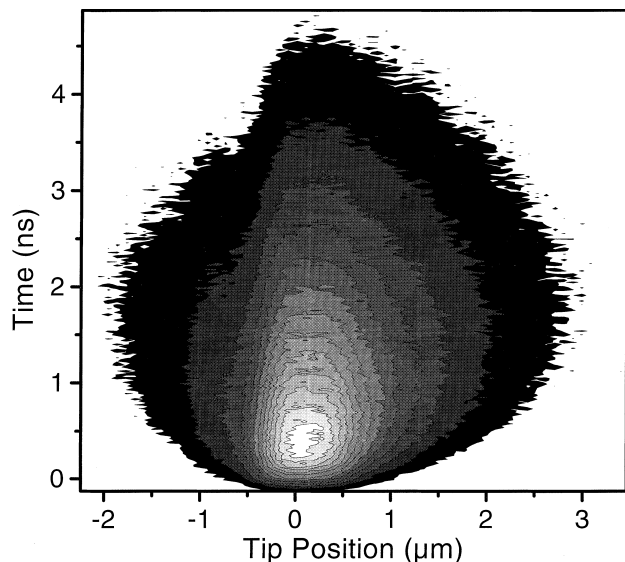


Fig. 3. Spatially and temporally resolved photoluminescence of the QWR at a temperature of 100K after localized excitation in the embedding quantum well (excitation energy 1.614 eV, detection energy 1.54 eV). The luminescence intensity is plotted as a function of the lateral distance y between excitation and QWR position and as a function of time.

respectively. In the insets of Fig. 4, these data are plotted on a logarithmic intensity scale. For excitation at $y = 0$, we find a rise of the QWR luminescence that is limited by the temporal resolution of our experiment of 260 ps and a decay of the QWR luminescence that is single exponential over two orders of magnitude with a decay time of 1.5 ns. This temporal dependence of the QWR luminescence remains unchanged for $|y| < 0.32 \mu\text{m}$, i.e. for excitation between the barriers separating QWR and embedding QW. For a distance $|y| > 0.32 \mu\text{m}$, the onset of the QWR luminescence is delayed with respect to that for excitation at $y = 0$. The rise of the QWR luminescence becomes monotonously slower with increasing $|y|$, as is highlighted in Fig. 5, where normalized QWR luminescence profiles for fixed excitation positions $y = 0, 0.9$ and $1.8 \mu\text{m}$ on the mesa top are compared. The delayed rise manifests itself in a shift of the maximum of the PL intensity in time with increasing y . The temporal position of the maximum PL intensity, t_{max} , remains constant, $t_{\text{max}} \approx 0.4 \text{ ns}$, for excitation at $|y| < 0.32 \mu\text{m}$, that is in between the barriers. For excitation outside the barriers, t_{max} increases almost linearly with increasing distance y , with a slope of $0.73 \text{ ns } \mu\text{m}^{-1}$ for $y < -0.32 \mu\text{m}$ and $0.62 \text{ ns } \mu\text{m}^{-1}$ for $y > 0.32 \mu\text{m}$. The maximum intensity of QWR luminescence after excitation on the mesa bottom ($y < 0$) is smaller than for mesa top ($y > 0$) excitation, i.e. fewer carriers are trapped into the QWR. This is evident from the amplitude values in Fig. 4(a) and (b) and from the shape of the plot in Fig. 3 at positive and negative y .

In the following, we discuss the luminescence behaviour

found for different excitation positions y . For $|y| < 0.32 \mu\text{m}$, the single exponential decay of the QWR PL gives a population lifetime of the QWR (Gershoni *et al.*, 1994, Akiyama *et al.*, 1994) of 1.5 ns, slightly longer than the PL decay time of the embedding QW of 1.35 ns. The slow single exponential decay of the QWR PL indicates the high structural quality of the QWR sample. The fast rise of the QWR PL after excitation at $|y| < 0.32 \mu\text{m}$ demonstrates that carrier relaxation from QW continuum states into localized QWR states occurs within the time resolution of the experiment of 260 ps. This relaxation involves both trapping into and energy relaxation within the QWR. For our very low excitation density of $\leq 10^5 \text{ cm}^{-2}$, carrier-carrier scattering is negligible and emission of longitudinal optical phonons represents the dominant process populating low-lying QWR states (Ryan *et al.*, 1996).

The onset of the QWR luminescence for excitation at $|y| > 0.32 \mu\text{m}$, i.e. for photogeneration of carriers in the QW, occurs with a delay of several hundred picoseconds. This delay increases with y (Fig. 3), reflecting the travelling time of carriers from the excited QW area to the QWR location. In our experiment, the optical excitation is resonant to the heavy hole exciton transition of the QW, which is about 10 meV below the onset of the band-to-band continuum. For a lattice temperature of 100K and weak excitation, real space transfer in the QW is dominated by excitonic transport (Hillmer *et al.*, 1992). This conclusion is supported strongly by independent time-resolved near-field experiments (not shown) monitoring the QW instead of the QWR emission. Here, at a fixed excitation position, the change in the decay of the QW emission is correlated directly with the corresponding rise of the QWR emission allowing us to rule out independent single-particle transport of electrons and holes. The time scale of transport is several hundred picoseconds, much longer than the formation and energy relaxation times of excitons, i.e. excitons undergoing real-space transfer form a quasi-equilibrium energy distribution close to the lattice temperature. In such a case, an isothermal drift-diffusion model is appropriate to describe the spatially resolved exciton dynamics. A purely diffusive transport model is clearly inappropriate as it does not account for: (i) the constant decay curves for $|y| < 0.32 \mu\text{m}$ and (ii) the strong difference in QWR PL intensities for mesa top and bottom excitation.

Such exciton transport is described by the two-dimensional particle current density $\vec{j}(\vec{r}, t) = \vec{j}_{\text{diff}}(\vec{r}, t) + \vec{j}_{\text{drift}}(\vec{r}, t)$ with a diffusion term $\vec{j}_{\text{diff}}(\vec{r}, t) = -D_{\text{ex}} \nabla n(\vec{r}, t)$ induced by the gradient of the exciton concentration $n(\vec{r}, t)$ ($\vec{r} = (x, y)$, D_{ex} : exciton diffusion coefficient) and a drift term $\vec{j}_{\text{drift}}(\vec{r}, t) = -\mu_{\text{ex}} n(\vec{r}, t) \nabla U(\vec{r})$ induced by the action of the local band gap gradient $\nabla U(\vec{r})$ on the centre of mass motion of the exciton (μ_{ex} : equivalent charged particle mobility of the exciton) (Tamor & Wolfe, 1980). Under the conditions of our experiment, μ_{ex} is linked to the diffusion coefficient D_{ex} by the

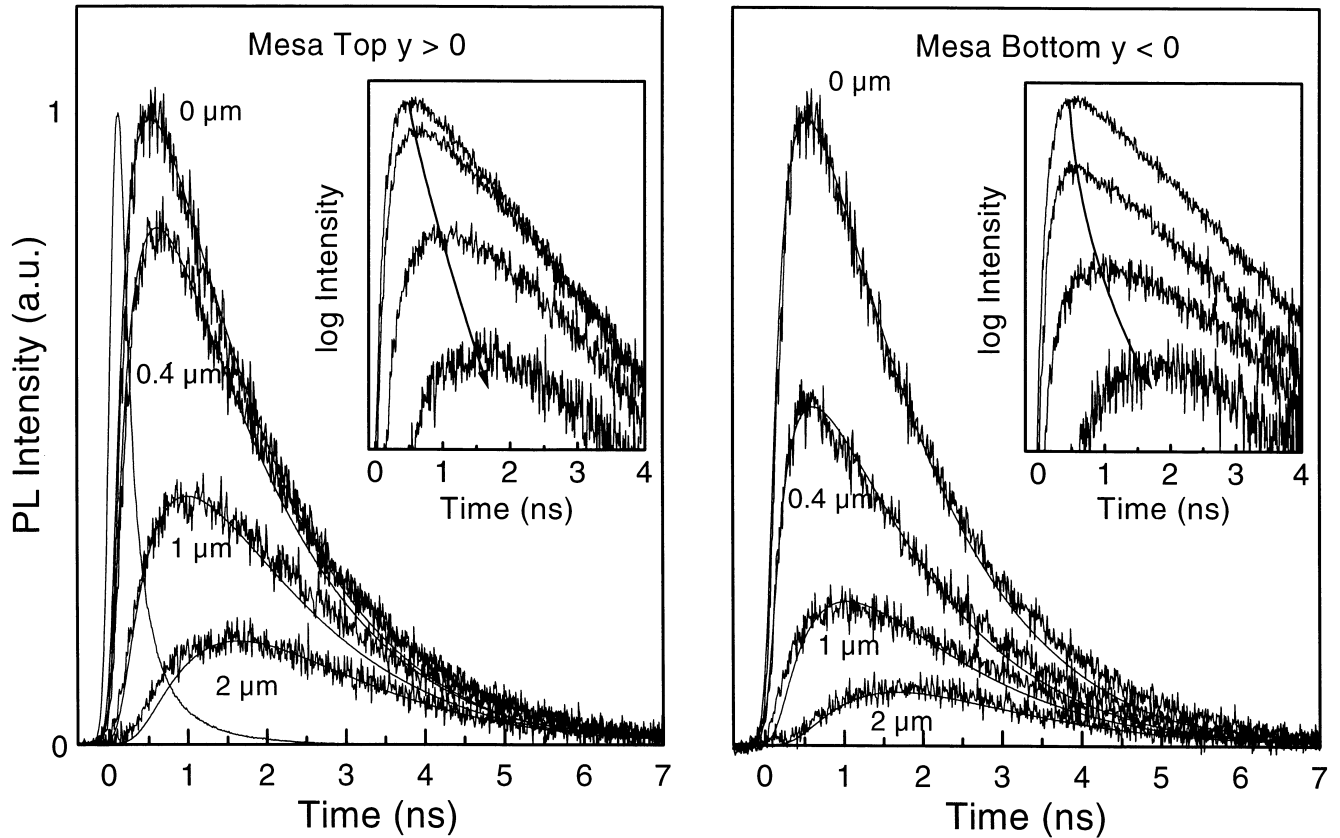


Fig. 4. Time evolution of QWR luminescence after excitation on the (a) mesa top and (b) mesa bottom of the QWR structure. The luminescence intensity at 1.54 eV is plotted vs. time for different excitation positions y and shows an increasingly delayed rise with increasing y which is due to the transport time of excitons from the excitation spot to the QWR. Shown as a solid line is the response function of the single photon counting detection. Insets: data plotted on a logarithmic intensity scale. Solid lines: results of a numerical calculation based on a drift-diffusion model for exciton transport.

Einstein relation $\mu_{ex} = eD_{ex}/kT$ (e = electron charge, k = Boltzmann constant). The spatio-temporal evolution of the exciton concentration $n(\vec{r}, t)$ is described by the two-dimensional continuity equation, including a generation, a diffusion, a drift, and a recombination term:

$$\frac{\partial n(\vec{r}, t)}{\partial t} = g(\vec{r}, \vec{r}_0, t) + D_{ex} \Delta n(\vec{r}, t) + \mu_{ex} \nabla n(\vec{r}, t) \cdot \nabla U(\vec{r}) - n(\vec{r}, t)/\tau(\vec{r}) \quad (1)$$

Here, the spatial variation of the band gap $U(\vec{r})$ along the lateral y direction, perpendicular to the wire axis, is directly taken from the confinement potential in Fig. 2. Note that $U(\vec{r})$ does not depend on the x coordinate, i.e. the direction parallel to the wire axis. The exciton lifetime $\tau(\vec{r})$ has a value of 1.5 ns for the QWR and 1.35 ns for the QW. For the generation term $g(\vec{r}, t)$, we use a Gaussian shape in time (FWHM of 1 ps) and space (FWHM of 300 nm) centred at $\vec{r} = (0, y)$. The intensity of the time-resolved QWR luminescence is proportional to $I(t) = \int dx \int dy \partial n(\vec{r}, t)/\partial t$, where the integration is performed over the length of the QWR along

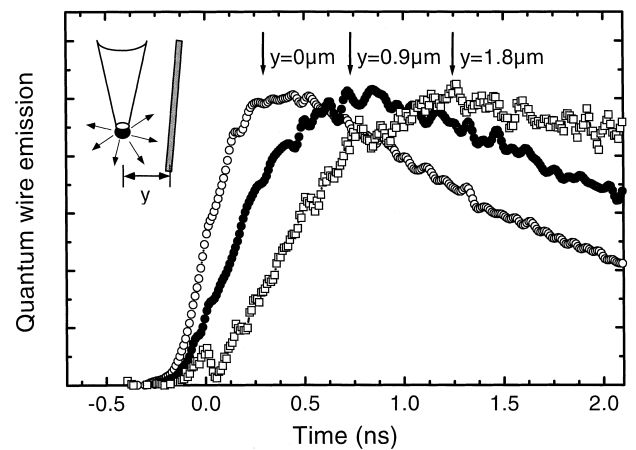


Fig. 5. Temporal profiles of the QWR luminescence for fixed excitation position y for mesa top excitation. Exciton transport within the GaAs QW from the generation point towards the QWR location causes a delayed rise of the QWR luminescence. The maximum of the QWR emission for each excitation position has been normalized to unity.

the x -axis and over the width of the QWR region along the y -axis. For comparison with experiment, $I(t)$ is convoluted with the temporal response function of the photodetector (solid line in Fig. 4(a)). In Fig. 4, the results of such simulations for different tip positions y are compared to the experimental results. Assuming an exciton diffusion coefficient $D_{ex} = 13 \text{ cm}^2 \text{ s}^{-1}$, the calculated temporal dependence of the QWR luminescence is in good agreement for excitation on both mesa top and bottom. This diffusion coefficient corresponds to an excitonic mobility $\mu_{ex} = 1500 \text{ cm}^2 \text{ V}^{-1} \text{ s}^{-1}$ in the QW, given mainly by the 2D hole mobility and limited in this temperature range by LO phonon scattering. In particular, the model calculation correctly describes the influence of the lateral band gap variation $U(\vec{r})$ on the exciton transport. In the region outside the barriers, $U(\vec{r})$ exerts a force on the excitonic centre of mass motion that opposes the diffusive real-space transfer towards the QWR. This is manifested in the experimental data as: (i) a significantly weaker QWR luminescence for mesa bottom ($y < -0.32 \mu\text{m}$) than mesa top ($y > 0.32 \mu\text{m}$) excitation due to the higher barrier on the mesa bottom, and (ii) a slight shift of the temporal position of the maximum of the QWR emission t_{max} to shorter delay times on the mesa top. Both on mesa top and bottom, the calculated t_{max} are in good agreement with the measured values (see Fig. 4), indicating that the exciton diffusion constants are similar on both sides of the QWR. In contrast, in the region inside the barriers, $|y| < 0.32 \mu\text{m}$, the bandgap variation $U(\vec{r})$ accelerates the exciton transport towards the

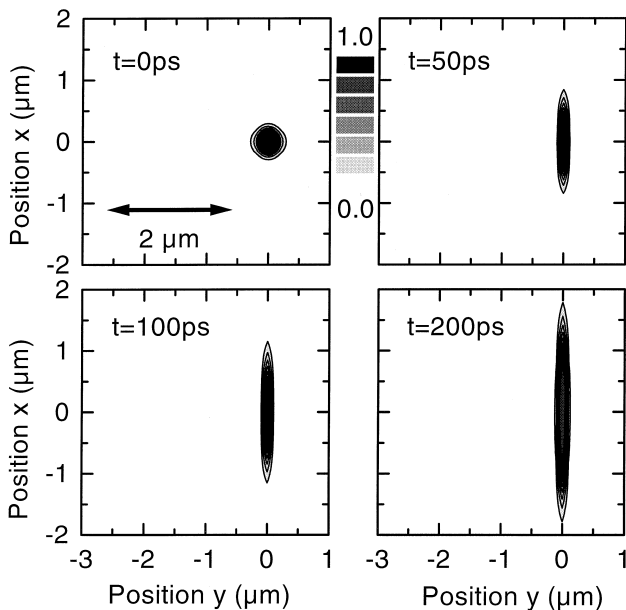


Fig. 6. Spatio-temporal evolution of the exciton density as calculated within the drift-diffusion model (Eq. (1)) for localized excitation at the QWR position, $y=0$. For each delay time, the maximum of the exciton density is normalized to 1.

wire, explaining directly the fast rise of the PL decay curve within the time resolution of the present experiment.

The quantitative agreement between model simulations and experiment makes us confident that the proposed classical excitonic drift-diffusion model provides a satisfactory description of the transport processes that are monitored in this experiment. To illustrate these dynamics more clearly, we show simulations of the full spatio-temporal evolution of the two-dimensional exciton density $n(\vec{r}, t)$ in Figs 6 and 7. The simulations are obtained by direct numerical integration of Eq. (1) with $\mu_{ex} = 1500 \text{ cm}^2 \text{ V}^{-1} \text{ s}^{-1}$, using a generation term $g(\vec{r}, t)$ as described above. For excitation at the QWR location, $y=0 \mu\text{m}$ (Fig. 6), the presence of the potential barriers leads to a rapid trapping of practically all generated excitons into the QWR, resulting in a spatial narrowing of the exciton distribution along the y -axis, perpendicular to the QWR axis. Diffusion of trapped QWR excitons results in a spreading of the QWR exciton distribution along the wire axis x . We note that, in these simulations, the exciton mobility along the wire axis was

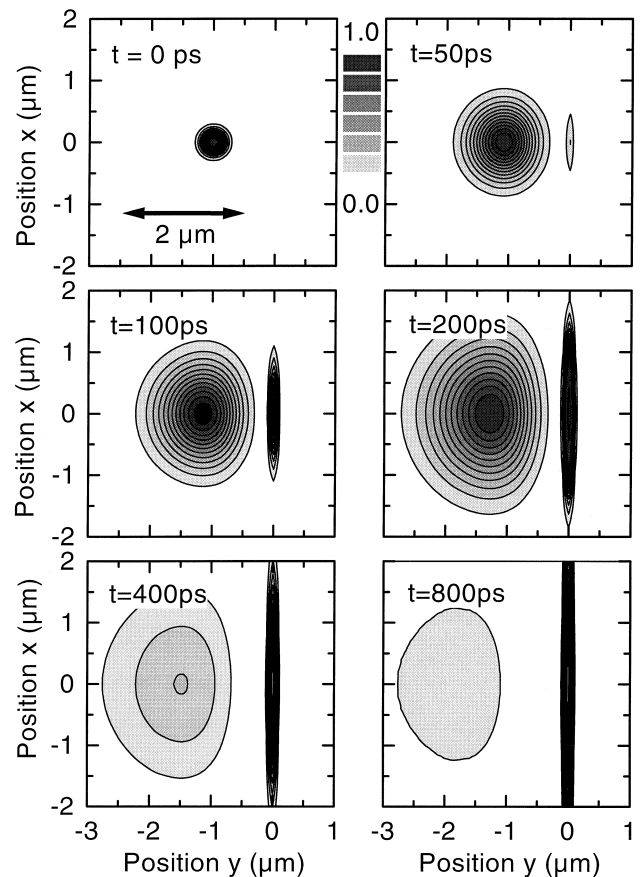


Fig. 7. Spatio-temporal evolution of the exciton density as calculated within the drift-diffusion model (Eq. (1)) for localized excitation at $y=-1 \mu\text{m}$ with respect to the QWR at $y=0$. For each delay time, the maximum of the exciton density is normalized to unity.

taken to be the same as the quantum well mobility, even though simplified theoretical models predict a higher 1D mobility due to a change in scattering rates (Sakaki, 1980). Near-field experiments allowing for an independent measurement of the 1D exciton mobility are currently underway in our laboratory. For excitation outside the barriers, e.g. at $y = -1 \mu\text{m}$ (Fig. 7), the initially narrow 2D exciton distribution spreads out within the QW plane. As observed experimentally, the build-up of QWR exciton population is delayed by roughly 100 ps and the QWR exciton population continues to increase within almost 1 ns, leading to a concomitant depletion of the QW exciton population.

We note that the influence of the drift current relative to the diffusion current becomes even more important at lower temperatures, where the ratio between barrier height and thermal energy increases. This is demonstrated in a similar time-resolved experiment at a lattice temperature of 10 K (Fig. 8). Again the sample is locally excited by transmitting femtosecond pulses that are resonant with the excitonic QW absorption band and time-resolved QW luminescence is detected at the peak of the QWR emission. At this temperature, QWR luminescence is only observed for excitation in a narrow region around $y = 0$. The intensity of the time-integrated QWR luminescence is found to

decrease monotonously with increasing separation of excitation tip and QWR. The spatial y -dependence of the time-integrated luminescence can be described by a Gaussian profile with a full width at half maximum of 570 nm. This width is more than twice the spatial resolution in the experiment that is independently determined by mapping the QWR luminescence for near-resonant QWR excitation. At each excitation position, the temporal dependence of the QWR luminescence can be described by a single exponential decay with a decay constant of 0.9 ns, the population lifetime of the QWR. No shift of the temporal position of the maximum PL intensity is observed within the accuracy of the experiment (± 50 ps). This indicates that at low temperature ($T = 10$ K) exciton transfer from outside the barriers is fully suppressed and that QWR luminescence is mainly observed for excitation between the maxima of the energetic barriers separating QWR and QW. The fact that we observe no temporal shift of the PL maximum suggests that, at this temperature, diffusive exciton transport is of minor importance for real-space transfer and trapping of excitons into the QWR.

Experiments at slightly higher temperatures, $T = 30$ K (Fig. 9(a)) and $T = 60$ K (Fig. 9(b)), highlight the influence of the asymmetry of the lateral bandgap variation on the

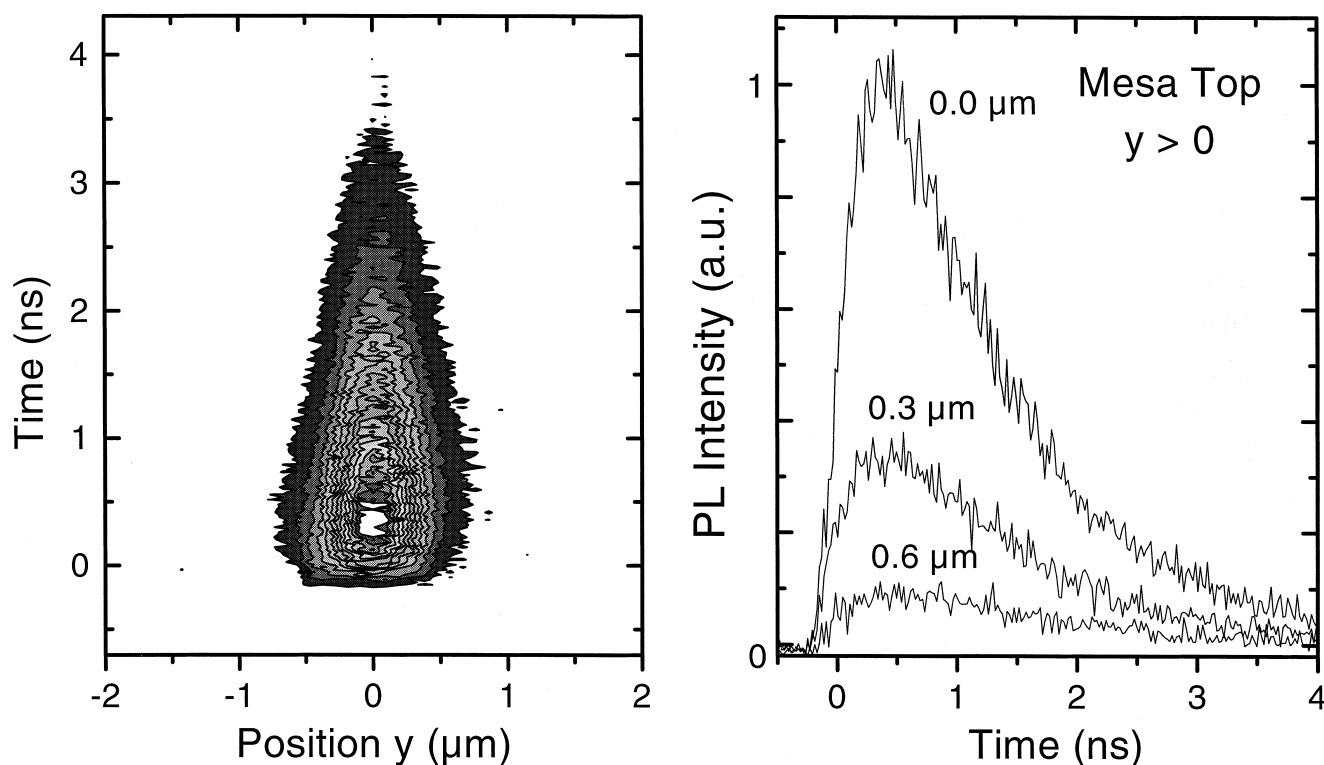


Fig. 8. (a) Temporally resolved QWR photoluminescence at a temperature of 10 K after localized excitation in the QW. Excitation conditions as in Fig. 3. The luminescence intensity is plotted as a function of the lateral distance y between excitation and QWR position and as a function of time. (b) Time evolution of the QWR luminescence after excitation on the mesa top. The luminescence intensity at 1.545 eV is plotted vs. time for different excitation positions.

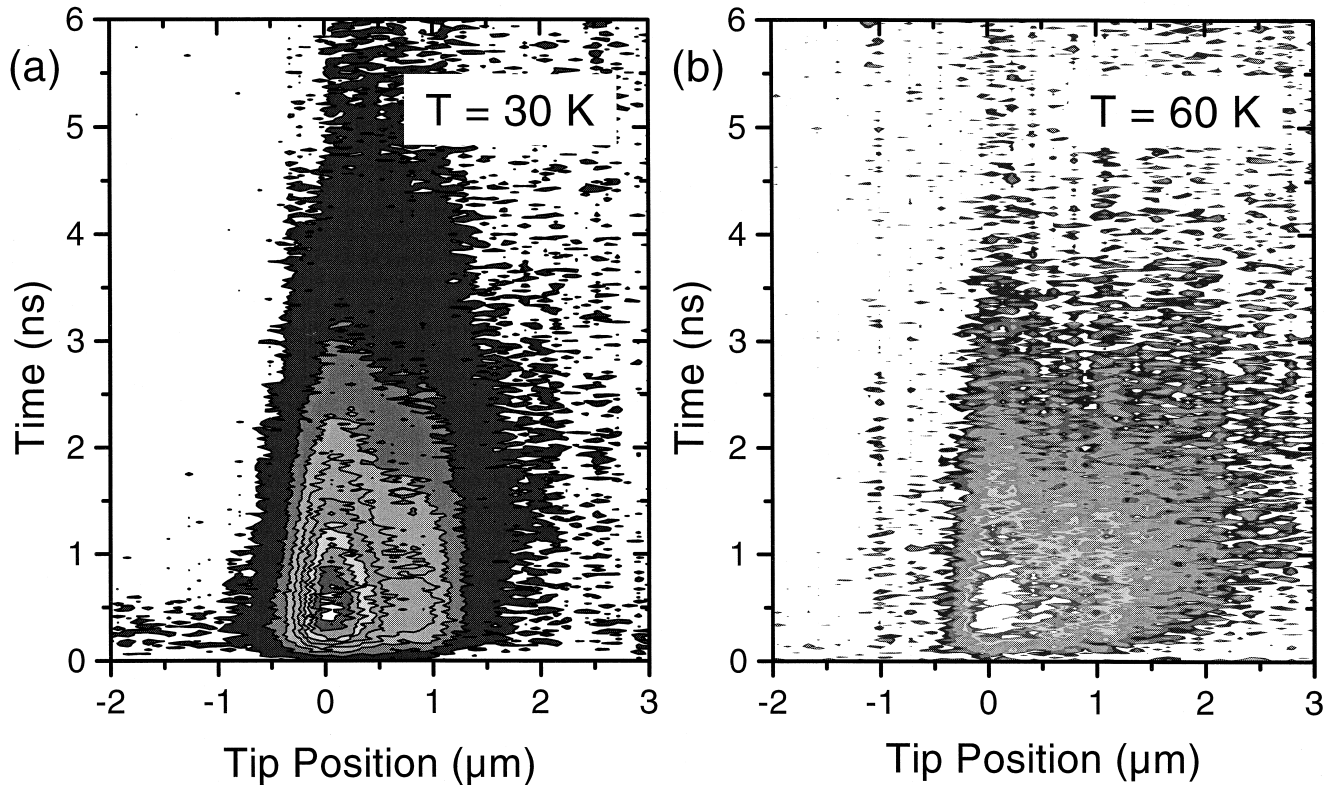


Fig. 9. As Fig. 8(a), for sample temperatures of (a) 30 K and (b) 60 K.

exciton transport into the wire. At both temperatures strong QWR luminescence is found for excitation around the QWR, $|y| < 0.4 \mu\text{m}$, showing a resolution-limited rise time. QWR luminescence is practically fully suppressed for mesa bottom excitation ($y < -0.4 \mu\text{m}$, high barrier), while the QWR luminescence intensity that is observed for excitation on the mesa top increases strongly with increasing temperature. A simulation of these experiments within the drift-diffusion

model discussed allows one to extract the quantum well exciton mobility (Fig. 10). At the lowest temperature of this study of 10 K, we find a QW mobility of $6000 \text{ cm}^2 \text{ V}^{-1} \text{ s}^{-1}$, in good agreement with results of previous experiments on (100) GaAs QWs (Hillmer *et al.*, 1989). In this temperature range, the exciton mobility is mainly limited by interface-roughness scattering (Hillmer *et al.*, 1993). Interface-roughness scattering rates decrease with increasing temperatures and this leads to an increase of the exciton mobility at temperatures of up to 50 K. At higher temperatures, acoustic-deformation potential scattering and polar-optical scattering (above 100 K) become dominant and result in the pronounced decrease of the exciton mobility with increasing temperature for $T > 50 \text{ K}$.

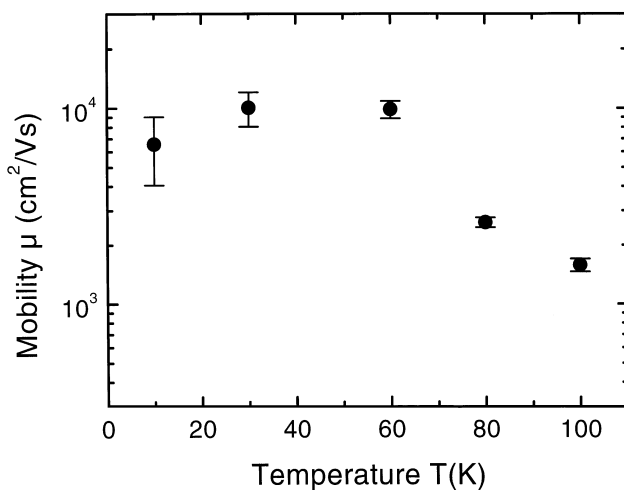


Fig. 10. QW exciton mobilities as a function of sample temperature as extracted from time-resolved near-field PL experiments.

Conclusion

Picosecond time-resolved near-field optical spectroscopy was used to study the exciton real-space transport in a novel GaAs quantum wire nanostructure. Studies over a wide temperature range from 10 to 100 K demonstrated the pronounced influence of local, subwavelength variations of the bandgap energy on the real-space exciton transport into single GaAs quantum wires. Such growth-correlated variations of the bandgap potential on a submicrometre length scale determine the carrier dynamics in a wide variety of low-dimensional semiconductor nanostructures

and time-resolved near-field spectroscopy presents a powerful tool for mapping these dynamics in both time and space.

Acknowledgement

Financial support by the Deutsche Forschungsgemeinschaft (SFB 296) is gratefully acknowledged.

References

- Akiyama, H., Koshiha, S., Someya, T., Wada, K., Noge, H., Nakamura, Y., Inoshita, T., Shimizu, A. & Sakaki, H. (1994) Thermalization effect on radiative decay of excitons in quantum wires. *Phys. Rev. Lett.* **72**, 924.
- Behme, G., Richter, A., Süptitz, M. & Lienau, C. (1997) Vacuum near-field scanning optical microscope for variable cryogenic temperatures. *Rev. Sci. Instrum.* **68**, 3458.
- Betzig, E. & Trautman, J.K. (1992) Near-field optics: microscopy, spectroscopy, and surface modification beyond the diffraction limit. *Science*, **257**, 189.
- Betzig, E., Trautman, J.K., Harris, T.D., Weiner, J.S. & Kostelak, R.L. (1991) Breaking the diffraction barrier: optical microscopy on a nanometric scale. *Science*, **251**, 1468.
- Gershoni, D., Katz, M., Wegscheider, W., Pfeiffer, L.N., Logan, R.A. & West, K. (1994) Radiative lifetimes of excitons in quantum wires. *Phys. Rev. B*, **50**, 8930.
- Hillmer, H., Forchel, A., Hansmann, S., Morohashi, M., Lopez, E., Maier, H.P. & Ploog, K.H. (1989) Optical investigations on the mobility of two-dimensional excitons in GaAs/Ga_{1-x}Al_xAs quantum wells. *Phys. Rev. B*, **39**, 10901.
- Hillmer, H., Forchel, A. & Tu, C.W. (1992) Enhancement of electron-hole pair mobilities in thin GaAs/Al_xGa_{1-x}As quantum wells. *Phys. Rev. B*, **45**, 1240.
- Hillmer, H., Forchel, A. & Tu, C.W. (1993) An optical study of the lateral motion of two-dimensional electron-hole pairs in GaAs/AlGaAs quantum wells. *J. Phys. Condens. Matter*, **5**, 5563.
- Levy, J., Nikitin, V., Kikkawa, J.M., Cohen, A., Samarth, N., Garcia, R. & Awschalom, D.D. (1996) Spatiotemporal near-field spin microscopy in patterned magnetic heterostructures. *Phys. Rev. Lett.* **76**, 1948.
- Lienau, Ch., Richter, A., Behme, G., Süptitz, M., Heinrich, D., Elsaesser, T., Ramsteiner, M., Nötzel, R. & Ploog, K.H. (1998) Nanoscale mapping of confinement potentials in single semiconductor quantum wires by near-field optical spectroscopy. *Phys. Rev. B*, **58**, 2045.
- Nötzel, R., Ramsteiner, M., Menniger, J., Trampert, A., Schönherr, H.-P., Däweritz, L. & Ploog, K.H. (1996) Micro-photoluminescence study at room temperature of sidewall quantum wires formed on patterned GaAs (311) A substrates by molecular beam epitaxy. *Jpn. J. Appl. Phys.* **35**, L297.
- Pohl, D.W., Denk, W. & Lanz, M. (1984) Optical stethoscopy: image recording with resolution $\lambda/20$. *Appl. Phys. Lett.* **44**, 651.
- Richter, A., Behme, G., Süptitz, M., Lienau, Ch., Elsaesser, T., Ramsteiner, M., Nötzel, R. & Ploog, K.H. (1997) Real-space transfer and trapping of carriers into single GaAs quantum wires studied by near-field optical spectroscopy. *Phys. Rev. Lett.* **79**, 2145.
- Ryan, J.F., Maciel, A.C., Kiener, C., Rota, L., Turner, K., Freyland, J.M., Marti, U., Martin, D., Morier-Gemoud, F. & Reinhart, F.K. (1996) Dynamics of electron capture into quantum wires. *Phys. Rev. B*, **53**, R4225.
- Sakaki, H. (1980) Scattering suppression and high-mobility effect of size-quantized electrons in ultrafine semiconductor wire structures. *Jpn. J. Appl. Phys.* **19**, L735.
- Stark, J.B., Mohideen, U., Betzig, E. & Slusher, R.E. (1996) Time-resolved nonlinear near-field optical microscopy of semiconductor microdisks. *Ultrafast Phenomena IX*, p. 349. Springer Series in Chemical Physics, Berlin.
- Tamor, M.A. & Wolfe, J.P. (1980) Drift and diffusion of free excitons in Si. *Phys. Rev. Lett.* **44**, 1703.